

Theoretical methods to design and test quantum simulators for the compact Abelian Higgs model

Yannick Meurice¹

¹ *Department of Physics and Astronomy, The University of Iowa, Iowa City, IA 52242 USA*

(Dated: July 26, 2021)

The lattice compact Abelian Higgs model is a non-perturbative regularized formulation of low-energy scalar quantum electrodynamics. In 1+1 dimensions, this model can be quantum simulated using a ladder-shaped optical lattice with Rydberg-dressed atoms [1]. In this setup, one spatial dimension is used to carry the angular momentum of the quantum rotors. One can use truncations corresponding to spin-2 and spin-1 to build local Hilbert spaces associated with the links of the lattice. We argue that ladder-shaped configurable arrays of Rydberg atoms can be used for the same purpose. We make concrete proposals involving two and three Rydberg atoms to build one local spin-1 space (a qutrit). We show that the building blocks of the Hamiltonian calculations are models with one and two spins. We compare target and simulators using perturbative and numerical methods. The two-atom setup provides an easily controllable simulator of the one-spin model while the three-atom setup involves solving nonlinear equations. This could be tested with current technology. We argue that near-term technology could be used to quantum simulate models with two or more spins.

I. INTRODUCTION

There has been recent interest in using quantum simulations and quantum computations to address problems with real-time and finite density in high-energy physics [2–11]. One initial step is the simulation of Abelian gauge theories [12, 13]. The Schwinger model introduces fermions and can be studied with methods developed in many-body physics [14–17]. Quantum simulations [18, 19] and quantum computations [20, 21] have been performed for this model.

A bosonic variant is the compact Abelian Higgs model. The compactness allows discrete character expansions formulations [22–24] which are gauge-invariant and solve [25] the questions of gauge redundancy and the implementation of Gauss’s law [26, 27]. The truncations do not break symmetries [24, 25, 28] but can affect the nature of phase transitions [29, 30]. An Optical lattice implementation with spin-2 has been proposed [1] in 1+1 dimensions. It is based on a ladder-shaped optical lattice with Rydberg-dressed atoms. In this setup, one spatial dimension carries the angular momentum of quantum rotors. Truncations corresponding to spin-2 and spin-1 local Hilbert spaces associated with the links of the lattice have been used.

In the following, we argue that ladder-shaped configurable arrays of Rydberg atoms [31–35], abbreviated CARA, can be used for the same purpose. This platform has been used for other lattice gauge theory models [36–38]. See Ref. [39] for a review of the use of Rydberg atoms. We make concrete proposals involving two and three Rydberg atoms to build one local spin-1 space (a qutrit). We show that the building blocks of the Hamiltonian calculations are simple models with one and two spins. We compare target and simulators for these models using perturbative and numerical methods. The two-atom setup provides an easily controllable simulator of the one-spin model while the three-atom setup involves

nonlinear matching. This could be tested with current technology. We argue that near-term technology could be used to quantum simulate models with two or more spins. More generally, programming with CARA amounts to a geometrical assembling allowing a broad range of applications. The idea of providing qutrits is very timely [40, 41].

The article is organized as follows. In Sec. II, we review the Lagrangian and Hamiltonian formulation of the compact Abelian Higgs model with emphasis on the meaning of the signs of the couplings. The general idea of ladder-shaped CARA is introduced in Sec. III. The two and three atoms CARA for a single spin-1 are discussed in Sec. IV. The coupling of two spins with an operator that is the product of their respective angular momentum L^z ’s is discussed in Sec. V. We argue that the single spin-1 simulators can be tested with current technology and that near-term technology could be used to quantum simulate models with two or more spins.

II. THE LATTICE MODEL

In this section we review the Lagrangian and Hamiltonian formulations of the compact Abelian Higgs model with emphasis on the meaning of the signs of the couplings. As we will see the sign question is important from the point of view of quantum simulations.

A. Lagrangian formulation

We first review the Lagrangian path integral formulation of the Abelian Higgs model at Euclidean time using most of the notations of Ref. [22] which should be consulted for more details. The partition function has the

form

$$Z = \int D\phi^\dagger D\phi DU e^{-S}. \quad (1)$$

The action is the sum of three terms

$$S = S_g + S_h + S_\lambda, \quad (2)$$

where the gauge part is

$$S_g = -\beta_{pl} \sum_x \text{Re} [U_{pl.,x}], \quad (3)$$

the hopping part

$$S_h = -\kappa_\tau \sum_x \left[\phi_x^\dagger U_{x,\hat{\tau}} \phi_{x+\hat{\tau}} + \phi_{x+\hat{\tau}}^\dagger U_{x,\hat{\tau}}^\dagger \phi_x \right] - \kappa_s \sum_x \left[\phi_x^\dagger U_{x,\hat{s}} \phi_{x+\hat{s}} + \phi_{x+\hat{s}}^\dagger U_{x,\hat{s}}^\dagger \phi_x \right], \quad (4)$$

and the self-interaction

$$S_\lambda = \lambda \sum_x (\phi_x^\dagger \phi_x - 1)^2 + \sum_x \phi_x^\dagger \phi_x. \quad (5)$$

By writing

$$\phi_x = |\phi_x| \exp(i\varphi_x), \quad (6)$$

we can separate the compact and non-compact variables in S_h :

$$S_h = -2\kappa_\tau |\phi_x| |\phi_{x+\hat{\tau}}| \sum_x \cos(\varphi_{x+\hat{\tau}} - \varphi_x + A_{x,\hat{\tau}}) - 2\kappa_s |\phi_x| |\phi_{x+\hat{s}}| \sum_x \cos(\varphi_{x+\hat{s}} - \varphi_x + A_{x,\hat{s}}). \quad (7)$$

It is assumed that κ_s and κ_τ are positive as in ferromagnetic interactions. This means that if we neglect the gauge fields and the self-interactions, large values of $|\phi|$ favor the alignment of the matter fields (configurations where all the angles φ_x are equal), as expected in the continuum limit of the free $O(2)$ scalar model.

In the following, we take the limit where λ become large and positive. The Brout-Englert-Higgs mode $|\phi|$ is then frozen to 1. The Nambu-Goldstone mode φ is compact. We call this model the compact Abelian Higgs model. By shifting the integration variable φ by π on every other site say in the spatial direction, we can flip the sign of κ_s without affecting the partition function. A similar reasoning can be applied for κ_τ and the time direction. However, if observable are inserted in the partition function, these changes of variable need to be performed for the observables. For instance, the magnetization becomes a staggered magnetization. Similar considerations apply to the plaquette term and the sign of β_{pl} . This is discussed at length in [42, 43].

B. Hamiltonian and Hilbert space

Following Ref. [1, 22, 23] the continuous-time limit for the compact Abelian Higgs model was taken in the field quantum number representation in the limit where the Higgs quartic self-coupling goes to infinity. To take the time continuum limit, one takes $\kappa_\tau, \beta_{pl} \rightarrow \infty$ while simultaneously taking κ_s , and the temporal lattice spacing, a , to zero such that the combinations

$$U \equiv \frac{1}{\beta_{pl}a} = \frac{g^2}{a}, \quad Y \equiv \frac{1}{2\kappa_\tau a}, \quad X \equiv \frac{2\kappa_s}{a} \quad (8)$$

are finite. These equations make clear that the signs of U , X and Y are the same as β_{pl} , κ_τ and κ_s respectively. The Hamiltonian for N_s links reads

$$H = \frac{U}{2} \sum_{i=1}^{N_s} (L_i^z)^2 + \frac{Y}{2} \sum_i' (L_{i+1}^z - L_i^z)^2 - X \sum_{i=1}^{N_s} U_i^x, \quad (9)$$

where the sum, \sum_i' , means that for open boundary conditions (OBC) we need to include $(L_1^z)^2 + (L_{N_s}^z)^2$. We used the operator

$$U^x \equiv \frac{1}{2}(U^+ + U^-), \quad (10)$$

with

$$U^\pm |m\rangle = |m \pm 1\rangle. \quad (11)$$

The quantum number m corresponds to the Fourier modes in the character expansion of the Lagrangian formulation [22]. In practice, we need to truncate The For a spin- m_{max} truncation we have

$$U^\pm |\pm m_{max}\rangle = 0 \quad (12)$$

In the following we mostly focus on the spin-1 truncation where $m = \pm 1, 0$. In this special case $U^x = L^x/\sqrt{2}$.

The truncations are compatible with the identities following from local or global symmetries of several models with continuous Abelian symmetries [24, 25, 28], however they can affect the type of phase transition present in the model.

The physical interpretation of the three terms of the Hamiltonian is the same as in conventional electrodynamics except for the fact that all the values involved are discrete. The U -term represents the electric field energy. The Y -term is associated with matter charges. They can be interpreted as charges determined by Gauss's law, in other words the difference between the two plaquettes (electric field) on each side of a site in the Lagrangian form. Finally the X -term is related to matter currents inducing temporal changes in the electric field, again in the Lagrangian form. This corresponds to the other inhomogeneous Maxwell equation involving the currents. In higher dimensions, the discrete curl of a magnetic field appears as in the continuum [25].

C. Charge conjugation

As in standard quantum electrodynamics this Hamiltonian has a charge conjugation symmetry. This will play an important role in the construction of simulators because this property will translate into a global reflection symmetry in the geometrical setup of the atoms. For this reason we remind the basic equations associated with this symmetry. The charge conjugation \mathcal{C} is a unitary transformation which reverses the sign of m :

$$\mathcal{C}|m\rangle = |-m\rangle \quad (13)$$

It is clear that $\mathcal{C}^2 = 1$ and that

$$\mathcal{C}L^z\mathcal{C}^{-1} = -L^z, \quad (14)$$

$$\mathcal{C}U^\pm\mathcal{C}^{-1} = U^\mp, \quad (15)$$

$$\mathcal{C}U^x\mathcal{C}^{-1} = U^x \quad (16)$$

This implies that the Hamiltonian is invariant under charge conjugation:

$$\mathcal{C}H\mathcal{C}^{-1} = H. \quad (17)$$

D. The building blocks of the Hamiltonian formalism

In order to conduct actual experiments to quantum simulate the compact Abelian Higgs model, we need to identify its building blocks. The first one is the local spin-1 or higher spin Hilbert space where we need to implement the operators L^z and U^x . This will be discussed in Sec. IV. The second is the coupling of two spins with an operator that is the product of their respective L^z 's. This will be discussed in Sec. V.

III. RYDBERG ATOM SIMULATORS

A. A ladder-shaped optical lattice simulator

In Ref. [1], a quantum simulator for the spin-2 truncation of the Hamiltonian in Eq. (9) was proposed. The general idea is to use an $5 \times N_s$ optical lattice that one can visualize as a ladder with N_s rungs. There is only one atom per rung and the five sites on each rung represent the 5 possible values for m with $m = 0$ at the center. Tunneling in the direction orthogonal to the rung is not allowed. Tunneling along the rung generates the X -term. The U -term is created with a parabolic potential. The Y -term is mediated by the $1/r^6$ interactions of the Rydberg-dressed atoms [44]. These interactions were chosen to be *attractive* and favoring ferromagnetism: neighbor atoms with the same m are closer to each other than atoms with different m 's. By taking the distance between the rungs a_s larger than the distance between the sites on the rungs

a_r , it is possible to do perturbation in a_r/a_s in Pythagoras theorem and approximately generate the quadratic Y -term. A more complete discussion and illustrations can be found in Ref. [1].

B. CARA simulators?

In the following we discuss the possibility of adapting the idea of Ref. [1] to configurable arrays of Rydberg atoms [31–35] denoted CARA. They can be configured by positioning ^{87}Rb atoms separated by controllable (but not too small) distances, homogeneously coupled to the excited Rydberg state $|r\rangle$ with a detuning Δ . The ground state is denoted $|g\rangle$ and the two possible states $|g\rangle$ and $|r\rangle$ can be seen as a qubit. The Hamiltonian reads

$$H = \frac{\Omega}{2} \sum_i (|g_i\rangle\langle r_i| + |r_i\rangle\langle g_i|) - \Delta \sum_i n_i + \sum_{i<j} V_{ij} n_i n_j, \quad (18)$$

with

$$V_{ij} = \Omega R_b^6 / r_{ij}^6, \quad (19)$$

for a distance r_{ij} between the atoms labelled as i and j . This repulsive interaction prevents two atoms close enough to each other to be in the $|r\rangle$ state. This is the so-called blockade mechanism.

This setup has been successfully used to simulate the Kibble-Zurek mechanism for chiral clock models [33]. It has been used to propose simulators for other gauge theories [36–38]. Simulations with Rydberg atoms are reviewed in Ref. [39].

In subsection III A, we discussed a setup [1] where one direction of the optical lattice was used to carry the $2S + 1$ spin degrees of freedom on the sites of the rungs. We will now try to replace each rung by a line of $2S + 1$ Rydberg atoms close enough to each other to prevent more than one atom to be in the $|r\rangle$ state. The spin-2 case is illustrated in Fig. 1. For instance, $m = 2$ corresponds to $|rgggg\rangle$. Also notice that charge conjugation is implemented by a reflection about the horizontal axis passing by the $m = 0$ states.

With current technology, it is difficult to get 5 atoms on a line close enough to make the blockade mechanism efficient. However it seems possible to do it with three atoms as in a spin-1 truncation. In the following we will concentrate on this simpler realization.

C. Spin-1 CARA implementations

For spin-1, we propose the correspondence

$$\begin{aligned} |1\rangle &\rightarrow |rgg\rangle, \\ |0\rangle &\rightarrow |grg\rangle, \\ |-1\rangle &\rightarrow |ggr\rangle. \end{aligned} \quad (20)$$

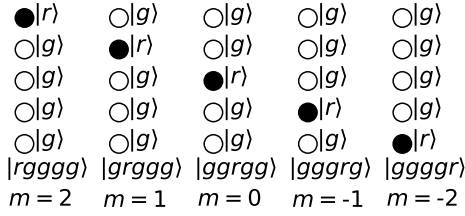


Figure 1. The 5 spin-2 states with a 5 atom setup.

This is illustrated in Fig. 2. Again, charge conjugation is implemented as a reflection with respect to the horizontal axis.

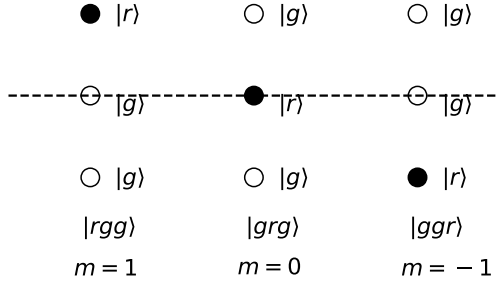


Figure 2. Three spin-1 states with the three atom setup, the 5 other possible states are not displayed.

An even simpler setup consists in using only two Rydberg atoms and having $|m=0\rangle$ to be a state without Rydberg states, namely

$$\begin{aligned} |1\rangle &\rightarrow |rg\rangle, \\ |0\rangle &\rightarrow |gg\rangle, \\ |-1\rangle &\rightarrow |gr\rangle. \end{aligned} \quad (21)$$

This is illustrated in Fig. 3. Since this second possibility is the simplest, it will be the starting point of the presentation of the next sections.

IV. ONE SPIN SYSTEM

In this section, we discuss the one spin-1 Hilbert space and the local Hamiltonian for the target model and the CARA implementations with two and three atoms.

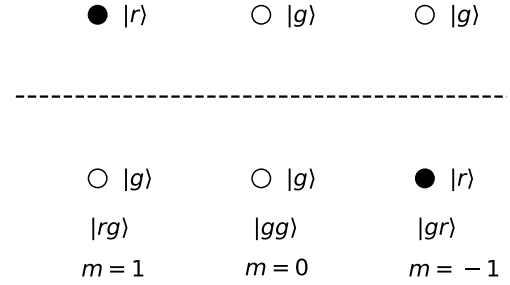


Figure 3. Spin-1 states with the two atom setup.

A. Target model

The local part of the target Hamiltonian is

$$H^{1T} = \frac{U}{2}(L^z)^2 - XU^x. \quad (22)$$

We will discuss the spectrum of this Hamiltonian with emphasis on the symmetries in order to build matching simulators. Since H^{1T} is invariant under charge conjugation, we introduce the \mathcal{C} eigenstates

$$|\pm\rangle \equiv \frac{1}{\sqrt{2}}(|1\rangle \pm |-1\rangle). \quad (23)$$

with \mathcal{C} -eigenvalues ± 1 :

$$\mathcal{C}|\pm\rangle = \pm|\pm\rangle. \quad (24)$$

They are also eigenstates of $(L^z)^2$ with eigenvalue 1. Note that

$$L^z|\pm\rangle = |\mp\rangle. \quad (25)$$

In addition $\mathcal{C}|0\rangle = |0\rangle$.

There is only one \mathcal{C} -odd state which is $|-\rangle$. It is annihilated by U^x

$$U^x|-\rangle = 0. \quad (26)$$

Consequently,

$$H^{1T}|-\rangle = \frac{U}{2}|-\rangle, \quad (27)$$

for any value of X .

In the \mathcal{C} -even sector, we have

$$U^x|0\rangle = \frac{1}{\sqrt{2}}|+\rangle, \quad (28)$$

$$U^x|+\rangle = \frac{1}{\sqrt{2}}|0\rangle, \quad (29)$$

and the eigenvalues are obtained from the even matrix in the $|0\rangle$, $|+\rangle$ basis:

$$H_{even}^{1T} = \begin{pmatrix} 0 & -\frac{X}{\sqrt{2}} \\ -\frac{X}{\sqrt{2}} & \frac{U}{2} \end{pmatrix} \quad (30)$$

The two eigenstates are

$$|0\rangle_X = \cos \phi |0\rangle + \sin \phi |+\rangle, \quad (31)$$

with eigenvalue

$$E_0(X) = \frac{1}{4}(U - \sqrt{U^2 + 8X^2}), \quad (32)$$

and

$$|+\rangle_X = \cos \phi |+\rangle - \sin \phi |0\rangle, \quad (33)$$

with eigenvalue

$$E_+(X) = \frac{1}{4}(U + \sqrt{U^2 + 8X^2}). \quad (34)$$

The mixing angle obeys the equation

$$\tan \phi = -\sqrt{2} \frac{E_0(X)}{X}. \quad (35)$$

If we treat X as a perturbation, we obtain that at the lowest nontrivial order

$$E_0(X) \simeq -\frac{X^2}{U}, \quad (36)$$

$$E_+(X) \simeq \frac{U}{2} + \frac{X^2}{U}, \quad (37)$$

$$\phi \simeq \sqrt{2} \frac{X}{U}. \quad (38)$$

These results can also be derived using standard perturbative formulas [45]. The perturbation has no diagonal element and the energy corrections occur at second order.

B. Two Rydberg atom implementation

The two atom setup discussed in Sec. III C provides a very simple implementation of a single spin-1 system. Introducing ± 1 labels for the top and bottom atoms, we call $n_{\pm 1}$ the occupation of their $|r\rangle$ state. The list of the possible states and their occupations are given in Table I. The Hamiltonian for the physical two-atom system is

$$H^{2R} = -\Delta(n_{+1} + n_{-1}) + V_0 n_{+1} n_{-1} \quad (39)$$

$$+ \frac{\Omega}{2} \sum_{\pm 1} (|g_{\pm 1}\rangle \langle r_{\pm 1}| + |r_{\pm 1}\rangle \langle g_{\pm 1}|). \quad (40)$$

We want to match this Hamiltonian with the target H^{1T} . We first consider the first term of the target Hamiltonian.

Setup	Ket	n_{+1}	n_{-1}	Short	Energy ($\Omega = 0$)
\bullet \circ	$ rg\rangle$	1	0	$ 1\rangle$	$-\Delta$
\circ \circ	$ gg\rangle$	0	0	$ 0\rangle$	0
\circ \bullet	$ gr\rangle$	0	1	$ -1\rangle$	$-\Delta$
\bullet \bullet	$ rr\rangle$	1	1	$ 2\rangle$	$-2\Delta + V_0$

Table I. Graphical representation of the two atoms in space, the symbol \circ represents the ground state $|g\rangle$ and \bullet the Rydberg state $|r\rangle$, ket notation, occupations, short notation and energy for $\Omega = 0$.

The splitting between $|0\rangle$ and $|\pm 1\rangle$ is $\frac{U}{2}$ when $\Omega = 0$, and can be implemented by setting

$$\Delta = -\frac{U}{2}. \quad (41)$$

In addition we want to suppress transitions to the $|rr\rangle$ state by introducing a large enough energy V_0 . This is the blockade mechanism. This can be achieved by positioning the two atoms close enough to each other.

In order to determine Ω , we compare the action of

$$H_1^{2R} = \frac{1}{2} \sum_{\pm 1} (|g_{\pm 1}\rangle \langle r_{\pm 1}| + |r_{\pm 1}\rangle \langle g_{\pm 1}|) \quad (42)$$

on the simulator Hilbert space to the action of U^x on the target Hilbert space.

$$H_1^{2R} |gg\rangle = \frac{1}{2} (|rg\rangle + |gr\rangle), \quad (43)$$

$$H_1^{2R} \frac{1}{\sqrt{2}} (|rg\rangle + |gr\rangle) = \frac{1}{\sqrt{2}} (|gg\rangle + |rr\rangle), \quad (44)$$

$$H_1^{2R} \frac{1}{\sqrt{2}} (|rg\rangle - |gr\rangle) = 0. \quad (45)$$

Comparing with the action of U^x on the three states of the target Hilbert space, we see that, except for the heavy state $|rr\rangle$, they are identical. Consequently, we can set

$$\Omega = -X. \quad (46)$$

Except for possible transitions to $|rr\rangle$, the correspondence is exact and the linear formula applies for arbitrary values of X . The good matching for $U = 1$ with $X = 0.5$ and $U = 1$ with $X = 1.5$ is demonstrated in Fig. 4.

C. Three Rydberg atom simulator

In the three atom setup, we have an additional atom which is associated with the $m = 0$ state. We label its

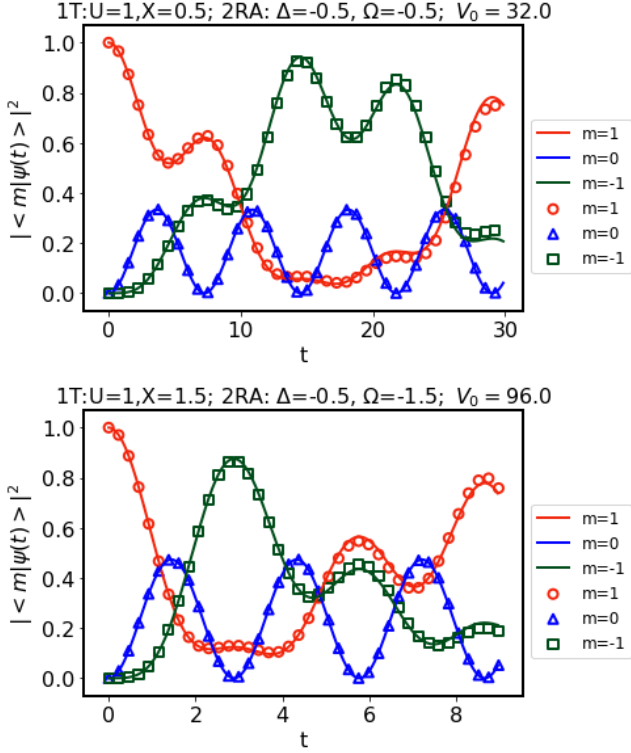


Figure 4. $|\langle m|U(t)|m=1\rangle|^2$, one site with exact Hamiltonian $U = 1$, $X = 0.5$ (solid lines) and Rydberg Hamiltonian with $\Omega = -0.5$, $\Delta = -0.5$ and $V_0 = 64|\Omega| = 32$ (empty symbols) (top), and $U = 1$, $X = 1.5$ (solid lines) and Rydberg Hamiltonian H^{2R} with $\Omega = -1.5$, $\Delta = -0.5$ and $V_0 = 64|\Omega| = 96$ (empty symbols) (bottom).

$|r\rangle$ occupation n_0 . The Hamiltonian reads

$$H^{3R} = -\Delta_0 n_0 - \Delta \sum_{j=0,\pm 1} n_j \quad (47)$$

$$+ V_0(n_0 n_{+1} + n_0 n_{-1}) + V'_0 n_{+1} n_{-1} \quad (48)$$

$$+ \frac{\Omega}{2} \sum_{j=0,\pm 1} (|g_j\rangle \langle r_j| + |r_j\rangle \langle g_j|), \quad (49)$$

with

$$V'_0 = \frac{V_0}{64} \quad (50)$$

when the three atoms are located equidistantly on a line as in Fig. 2. The spin-1 sector is shown in Table II. The auxiliary sector has five states shown in Table III. Following previous notation, we also define

$$|\pm'\rangle \equiv \frac{1}{\sqrt{2}}(|1'\rangle \pm |-1'\rangle), \quad (51)$$

and

$$H_1^{3R} = \frac{1}{2} \sum_{j=0,\pm 1} (|g_j\rangle \langle r_j| + |r_j\rangle \langle g_j|), \quad (52)$$

Setup	Ket	Energy ($\Omega = 0$)
• ○ ○	$ 1\rangle$	$-\Delta$
○ • ○	$ 0\rangle$	$-\Delta - \Delta_0$
○ ○ •	$ -1\rangle$	$-\Delta$

Table II. Spin-1 states for the three atom simulator.

Setup	Ket	Energy ($\Omega = 0$)
○ ○ ○	$ 0''\rangle$	0
• • ○	$ 1'\rangle$	$-2\Delta - \Delta_0 + V_0$
• ○ •	$ 0'\rangle$	$-2\Delta + \frac{V_0}{64}$
○ • •	$ -1'\rangle$	$-2\Delta - \Delta_0 + V_0$
• • •	$ 3\rangle$	$-3\Delta - \Delta_0 + 2V_0 + \frac{V_0}{64}$

Table III. Auxiliary states for the three atom simulator.

Unlike the previous situation with two atoms, H_1^{3R} only connects the spin-1 sector with the auxiliary sector

$$H_1^{3R} |0\rangle = \frac{1}{2} |0''\rangle + \frac{1}{\sqrt{2}} |+\rangle, \quad (53)$$

$$H_1^{3R} |+\rangle = \frac{1}{2} |+\rangle + \frac{1}{\sqrt{2}} |0'\rangle + \frac{1}{\sqrt{2}} |0''\rangle, \quad (54)$$

$$H_1^{3R} |-\rangle = \frac{1}{2} |-\rangle. \quad (55)$$

Using the corresponding matrix elements together with standard perturbation theory [45], we obtain the perturbative matching equation for the energy differences:

$$\frac{X^2}{U} = \frac{\Omega^2}{2} \left(\frac{1}{\Delta - \frac{V_0}{64}} - \frac{1}{\Delta} \right), \quad (56)$$

$$\frac{U}{2} + \frac{X^2}{U} = \Delta_0 + \frac{\Omega^2}{4} \left(\frac{1}{\Delta + \Delta_0} + \frac{2}{V_0 - \Delta} - \frac{1}{V_0 - \Delta - \Delta_0} \right).$$

Similarly we can try to match perturbative expressions for the mixing angle ϕ defined in Eq. (35). However, ϕ contributions appear at first order in X in the target model (because U^x connects $|0\rangle$ and $|+\rangle$), but only at

second order in Ω in the three-atom simulator. More explicitly,

$$\sqrt{2}\frac{X}{U} = \frac{\Omega^2}{2\sqrt{2}\Delta_0} \left(\frac{1}{\Delta + \Delta_0} + \frac{1}{V_0 - \Delta} \right). \quad (57)$$

This apparently contradicts the idea that X and Ω should be proportional for small values of X . If we are given U and X , we have three nonlinear equations for Ω , Δ , Δ_0 and V_0 and generically, we expect one-parameter families of solutions. By fixing one of the unknowns, one can look for solutions using Newton's method. More generally, it is easy to find accurate numerical solutions for the energies and mixing of the simulators and it seems possible to attack the matching problem non perturbatively. In order to pursue such effort, it would be useful to know the range of values corresponding to feasible experiments.

With today's technology, it seems difficult to create non homogeneous detuning and we should consider the limit where Δ_0 is zero. In this limit, $|0\rangle$ and $|+\rangle$ are degenerate when Ω is set to zero. In the $|0\rangle$ and $|+\rangle$ basis, the energy matrix up to second order in Ω has the form

$$-\Delta \mathbb{1} - \frac{\Omega^2}{4} \mathbb{M},$$

with

$$\mathbb{M} = \begin{pmatrix} \frac{1}{\Delta} + \frac{2}{V_0 - \Delta} & \frac{\sqrt{2}}{\Delta} + \frac{\sqrt{2}}{V_0 - \Delta} \\ \frac{\sqrt{2}}{\Delta} + \frac{\sqrt{2}}{V_0 - \Delta} & \frac{2}{\Delta} + \frac{1}{V_0 - \Delta} - \frac{2}{\Delta - \frac{V_0}{64}} \end{pmatrix}. \quad (58)$$

The matrix \mathbb{M} determines the mixing angle and the eigenvalues.

D. An example of approximate solution with three Rydberg atoms

The three-atom simulator leads to nonlinear equations. However, it is not difficult to find approximate solutions when Δ and V_0 are in a specific ratio. As a simple example, we picked

$$\Delta_0 = 0 \text{ and } V_0 = 2\Delta. \quad (59)$$

If we neglect the $\frac{V_0}{64}$ term, we have

$$\mathbb{M} \simeq \frac{1}{\Delta} \begin{pmatrix} 3 & 2\sqrt{2} \\ 2\sqrt{2} & 1 \end{pmatrix}. \quad (60)$$

Given that there is an overall minus sign in front of \mathbb{M} , its largest eigenvalue corresponds to the lowest energy state and the mixing angle approximately satisfies the equation

$$\tan \phi \simeq \frac{1}{\sqrt{2}} \quad (61)$$

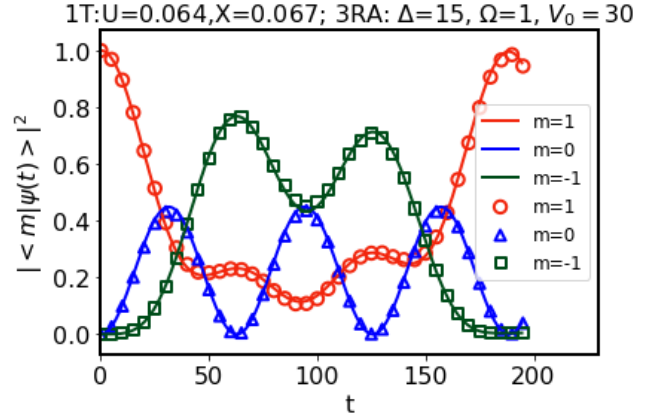


Figure 5. $|\langle m|U(t)|m=1\rangle|^2$ for one site with exact Hamiltonian $U = 0.064$, $X = 0.067$ (solid lines), Rydberg Hamiltonian with $\Omega = 1$, $\Delta = 15$ and $V_0 = 30$ (empty symbols).

Comparing with Eq. (35), we find that this angle corresponds to the situation $X = U$. Furthermore, we can compute the energy spectrum in this simple example. The eigenvalues of \mathbb{M} are approximately $5/\Delta$ and $-1/\Delta$. In addition, we have up to second order in Ω :

$$E_- = -\Delta - \frac{\Omega^2}{4} \frac{1}{V_0 - \Delta}. \quad (62)$$

Consequently, in this simple example, we have

$$E_+ - E_0 = \frac{3}{2} \frac{\Omega^2}{\Delta}, \quad (63)$$

$$E_- - E_0 = \frac{\Omega^2}{\Delta}. \quad (64)$$

In the target model with $X = U$, we have

$$E_+ - E_0 = \frac{3}{2} U, \quad (65)$$

$$E_- - E_0 = U. \quad (66)$$

The ratio of differences are both $3/2$ and we can match the scale for $\Omega^2/\Delta = U$. Given that the matrix has been approximated, we should look for matching in the region $X \simeq U$. As a numerical example, we used $\Omega = 1$, $\Delta = 15$ and $V_0 = 30$ and found good matching for $U = 0.064$, $X = 0.067$ both close to $1/15 = 0.0666\dots$. This is illustrated in Fig. 5.

V. TWO-SPIN SYSTEM

In this section, we follow the same sequence as in Sec. IV for a two-spin system motivated by the Hamiltonian of Eq. (9).

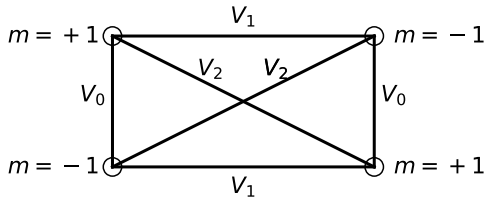


Figure 6. Rydberg interactions for the four atom simulator.

A. Target model

For the target model we consider two spins called left (L) and right (R) connected by a Y -term. The target Hamiltonian for the two-spin system is chosen to be

$$\begin{aligned} H^{2T} &= H_L^{1T} + H_R^{1T} + \frac{Y}{2}(L_L^z - L_R^z)^2 \\ &= \frac{U}{2}((L_L^z)^2 + (L_R^z)^2) - X(U_R^x + U_L^x) + \frac{Y}{2}(L_L^z - L_R^z)^2 \end{aligned} \quad (67)$$

We focus on a special target situation where solutions of the one-spin problems are available, more specifically we picked $U = 1$, $X = 1.2$ and $Y = 0.2$. For the time evolution we consider an initial state $|0, 0\rangle$, and calculate the probability to stay in that state or to be in the state

$$|S\rangle \equiv \frac{1}{2}(|0, 1\rangle + |0, -1\rangle + |1, 0\rangle + |-1, 0\rangle). \quad (68)$$

obtained by applying the X -term on the initial state. This guarantees a significant overlap when X is not too small.

B. Four Rydberg atom simulator

For a simulator with four atoms, we use the two-atom setup for two pairs and include the additional V_{ij} appearing in Eq. (18). The Hamiltonian reads

$$\begin{aligned} H^{4R} &= H_L^{2R} + H_R^{2R} \\ &+ V_1(n_{+1L}n_{-1R} + n_{-1L}n_{+1R}) \\ &+ V_2(n_{+1L}n_{+1R} + n_{-1L}n_{-1R}) \end{aligned} \quad (69)$$

When the V_i are positive, we need to have the opposite signs closer (bipartite charge conjugations on alternate sites). In other words, if the interactions are repulsive and decreasing like $1/r^6$ we need to put the same m atoms farther apart. This is illustrated in Fig. 6. For the standard $1/r^6$ Rydberg interactions as in Eq. (19), and using

a_r and a_s as the vertical (as in one spin) and horizontal (coupling the two spins) lattice spacings respectively, and their ratio

$$\rho \equiv \frac{a_r}{a_s}, \quad (70)$$

we have

$$V_1 = V_0 \rho^6, \quad (71)$$

$$V_2 = V_0(\rho/\sqrt{1+\rho^2})^6. \quad (72)$$

The matching condition when $X = \Omega = 0$ reads

$$\Delta = -\frac{U}{2} - \frac{Y}{2}, \quad (73)$$

$$V_1 = Y, \quad (74)$$

$$V_2 = -Y. \quad (75)$$

The second equation can be solved using

$$\rho = \left(\frac{Y}{V_0}\right)^{1/6}. \quad (76)$$

The third equation has no solutions for positive V_2 . In Eq. (71) V_2 is smaller than V_1 but nevertheless positive. This implies that it is not possible to exactly match the energy of the states $|+1, -1\rangle$ and $|-1, +1\rangle$. The possible solutions to this problem are: 1) ask experimentalists to adjust the couplings locally, 2) try to use the nonlinear effects in Ω to reduce the error or focus on the six-atom setup discussed below where we will see that the matching in the limit $\Omega = X = 0$ is approximately possible following the mechanism invoked in Ref. [1]. In order to give an idea of the size of the effects, we have considered the problem discussed in the target section, first with the futuristic $V_2 = -Y$ (the agreement is excellent) and then with today's technology and V_2 as in Eq. (71). The results are displayed in Fig. 7.

C. Six Rydberg atom implementation

We now consider a six-atom setup with two three-atom spin-1 setups. The Hamiltonian reads

$$\begin{aligned} H^{6R} &= H_L^{3R} + H_R^{3R} \\ &+ V_1(n_{+1L}n_{-1R} + n_{-1L}n_{+1R}) \\ &+ V_2(n_{0L}(n_{+1R} + n_{-1R})) \\ &+ V_2((n_{+1L} + n_{-1L})n_{0R}) \\ &+ V_3(n_{+1L}n_{+1R} + n_{-1L}n_{-1R}) \end{aligned} \quad (77)$$

When the V_i are positive, we again need to have the opposite signs closer. This is illustrated in Fig. 8. For the standard Rydberg interactions of Eq. (19), we have V_1 and V_2 as in Eq. (71) and

$$V_3 = V_0(\rho/\sqrt{1+4\rho^2})^6 \quad (78)$$

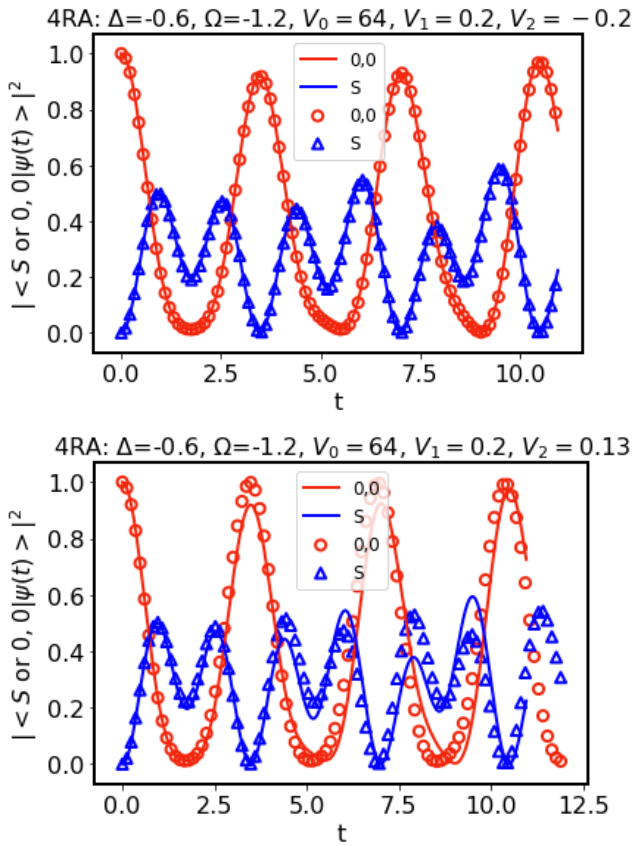


Figure 7. $|\langle 0,0|U(t)|0,0\rangle|^2$ and $|\langle S|U(t)|0,0\rangle|^2$, with $|S\rangle$ defined in Eq. (68), for the target two-spin Hamiltonian with $U = 1$, $X = 1.2$ and $Y = 0.2$ (solid lines) and the four atom simulator with $\Delta=-0.6$, $\Omega=-1.2$, $V_0 = 64$, $V_1 = 0.2$, with $V_2 = -0.2$ (top) and $V_2 = 0.13$ (bottom).

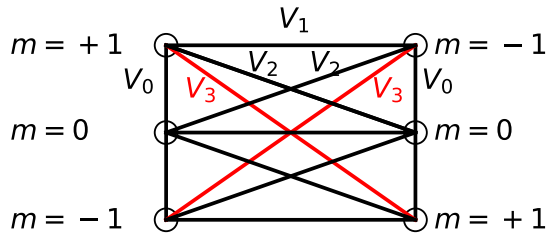


Figure 8. Rydberg interactions for the six atom simulator.

Matching condition when $X = \Omega = 0$ are

$$\begin{aligned}\Delta_0 &= \frac{U}{2} + Y \\ V_1 - V_2 &= \frac{Y}{2} \\ V_1 - V_3 &= 2Y,\end{aligned}\quad (79)$$

These equations have approximate solutions for a tuned ρ when Y is not too large. In Fig. $\Delta=15$, $\Omega=1$, $V_0 = 30$, $\rho=0.326$. A rescaling $K = 0.05464$ has been applied to

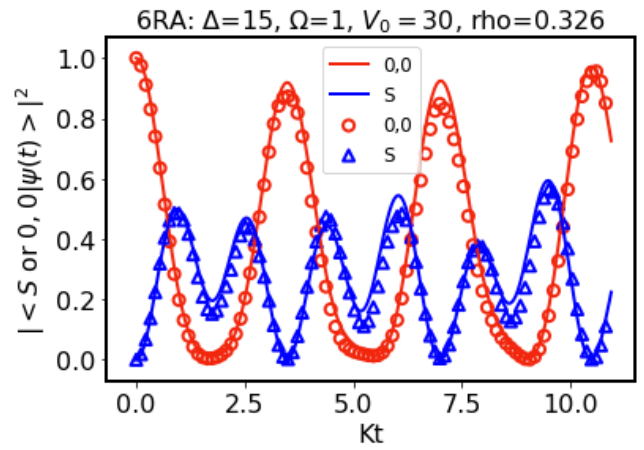


Figure 9. $|\langle 0,0|U(t)|0,0\rangle|^2$ and $|\langle S|U(t)|0,0\rangle|^2$, with $|S\rangle$ defined in Eq. (68), with the target two-spin Hamiltonian with $U = 1$, $X = 1.2$ and $Y = 0.2$ (solid lines) and the six atom simulator with $\Delta=15$, $\Omega=1$, $V_0 = 30$, $\rho=0.326$. A rescaling $K = 0.05464$ has been applied to the simulator time to match the target evolution.

the simulator time to match the target evolution. In Fig. 9, we show the case $\Delta=15$, $\Omega=1$, $V_0 = 30$, as in the one spin-1, with $\rho=0.326$. A rescaling $K = 0.05464$ has been applied to the simulator time to match the target evolution.

VI. CONCLUSIONS

In summary, we have proposed ladder-shaped CARA with two and three atoms for a single spin-1 and four and six atoms for two coupled spins. In one spatial dimension this is all we need to control. We compared target and simulators using perturbative and numerical methods. The two-atom setup provides an easily controllable simulator of the one-spin model while the three-atom setup involves a nonlinear matching. This could be tested with current technology. We argue that near-term technology could be used to quantum simulate models with two or more spins.

Acknowledgments. This work is supported in part by the U.S. Department of Energy (DoE) under Award Number DE-SC0019139. Special thanks to Alex Keesling who enthusiastically supported the idea using the Rabi driven tern to replace the tunneling in the original for-

mulation and made very interesting suggestions. We also thank Shan-wen Tsai, Jin Zhang, James Corona, Erik Gustafson, Denis Candido, Michael Flatte, Craig Pryor, Nate Gemelke, Tout Wang, Shangtao Wang and the members of QuLAT for suggestions and comments.

-
- [1] J. Zhang, J. Unmuth-Yockey, J. Zeiher, A. Bazavov, S. W. Tsai, and Y. Meurice, *Phys. Rev. Lett.* **121**, 223201 (2018), arXiv:1803.11166 [hep-lat].
- [2] M. C. Bañuls, R. Blatt, J. Catani, A. Celi, J. I. Cirac, M. Dalmonte, L. Fallani, K. Jansen, M. Lewenstein, S. Montangero, C. A. Muschik, B. Reznik, E. Rico, L. Tagliacozzo, K. Van Acoleyen, F. Verstraete, U.-J. Wiese, M. Wingate, J. Zakrzewski, and P. Zoller, *European Physical Journal D* **74**, 165 (2020), arXiv:1911.00003 [quant-ph].
- [3] N. Klco, A. Roggero, and M. J. Savage, (2021), arXiv:2107.04769 [quant-ph].
- [4] M. Aidelsburger *et al.*, (2021), arXiv:2106.03063 [cond-mat.quant-gas].
- [5] U.-J. Wiese, (2021), arXiv:2107.09335 [hep-lat].
- [6] E. Gustafson, Y. Zhu, P. Dreher, N. M. Linke, and Y. Meurice, (2021), arXiv:2103.06848 [hep-lat].
- [7] H. Lamm, S. Lawrence, and Y. Yamauchi (NuQS), *Phys. Rev. D* **100**, 034518 (2019), arXiv:1903.08807 [hep-lat].
- [8] E. J. Gustafson and H. Lamm, *Phys. Rev. D* **103**, 054507 (2021), arXiv:2011.11677 [hep-lat].
- [9] R. C. Brower, D. Berenstein, and H. Kawai, *PoS LATTICE2019*, 112 (2020), arXiv:2002.10028 [hep-lat].
- [10] E. Zohar, J. I. Cirac, and B. Reznik, *Rept. Prog. Phys.* **79**, 014401 (2016), arXiv:1503.02312 [quant-ph].
- [11] U.-J. Wiese, *Annalen Phys.* **525**, 777 (2013), arXiv:1305.1602 [quant-ph].
- [12] E. Zohar and B. Reznik, *Phys. Rev. Lett.* **107**, 275301 (2011), arXiv:1108.1562 [quant-ph].
- [13] L. Tagliacozzo, A. Celi, A. Zamora, and M. Lewenstein, *Annals Phys.* **330**, 160 (2013), arXiv:1205.0496 [cond-mat.quant-gas].
- [14] M. C. Bañuls, K. Cichy, K. Jansen, and J. I. Cirac, *JHEP* **11**, 158 (2013), arXiv:1305.3765 [hep-lat].
- [15] B. Buyens, J. Haegeman, H. Verschelde, F. Verstraete, and K. Van Acoleyen, *Phys. Rev. X* **6**, 041040 (2016), arXiv:1509.00246 [hep-lat].
- [16] M. C. Bañuls, K. Cichy, K. Jansen, and H. Saito, *Phys. Rev. D* **93**, 094512 (2016), arXiv:1603.05002 [hep-lat].
- [17] L. Funcke, K. Jansen, and S. Kühn, *Phys. Rev. D* **101**, 054507 (2020), arXiv:1908.00551 [hep-lat].
- [18] E. A. Martinez *et al.*, *Nature* **534**, 516 (2016), arXiv:1605.04570 [quant-ph].
- [19] V. Kasper, F. Hebenstreit, F. Jendrzejewski, M. K. Oberthaler, and J. Berges, *New J. Phys.* **19**, 023030 (2017), arXiv:1608.03480 [cond-mat.quant-gas].
- [20] N. Klco, E. F. Dumitrescu, A. J. McCaskey, T. D. Morris, R. C. Pooser, M. Sanz, E. Solano, P. Lougovski, and M. J. Savage, *Phys. Rev. A* **98**, 032331 (2018), arXiv:1803.03326 [quant-ph].
- [21] D. E. Kharzeev and Y. Kikuchi, *Phys. Rev. Res.* **2**, 023342 (2020), arXiv:2001.00698 [hep-ph].
- [22] A. Bazavov, Y. Meurice, S.-W. Tsai, J. Unmuth-Yockey, and J. Zhang, *Phys. Rev.* **D92**, 076003 (2015), arXiv:1503.08354 [hep-lat].
- [23] J. Unmuth-Yockey, J. Zhang, A. Bazavov, Y. Meurice, and S.-W. Tsai, *Phys. Rev.* **D98**, 094511 (2018), arXiv:1807.09186 [hep-lat].
- [24] Y. Meurice, R. Sakai, and J. Unmuth-Yockey, (2020), arXiv:2010.06539 [hep-lat].
- [25] Y. Meurice, *Phys. Rev. D* **102**, 014506 (2020), arXiv:2003.10986 [hep-lat].
- [26] J. F. Unmuth-Yockey, *Phys. Rev. D* **99**, 074502 (2019), arXiv:1811.05884 [hep-lat].
- [27] J. Bender and E. Zohar, *Phys. Rev. D* **102**, 114517 (2020), arXiv:2008.01349 [quant-ph].
- [28] Y. Meurice, *Phys. Rev. D* **100**, 014506 (2019), arXiv:1903.01918 [hep-lat].
- [29] J. Zhang, Y. Meurice, and S.-W. Tsai, *Phys. Rev. B* **103**, 245137 (2021), arXiv:2104.06342 [cond-mat.quant-gas].
- [30] L. Hostetler, J. Zhang, R. Sakai, J. Unmuth-Yockey, A. Bazavov, and Y. Meurice, (2021), arXiv:2105.10450 [hep-lat].
- [31] H. Bernien, S. Schwartz, A. Keesling, H. Levine, A. Omran, H. Pichler, S. Choi, A. S. Zibrov, M. Endres, M. Greiner, V. Vuletić, and M. D. Lukin, *Nature (London)* **551**, 579 (2017), arXiv:1707.04344 [quant-ph].
- [32] M. Endres, H. Bernien, A. Keesling, H. Levine, E. R. Anschuetz, A. Krajenbrink, C. Senko, V. Vuletic, M. Greiner, and M. D. Lukin, *Science* **354**, 1024 (2016).
- [33] A. Keesling *et al.*, *Nature* **568**, 207 (2019), arXiv:1809.05540 [quant-ph].
- [34] I. Cong, S.-T. Wang, H. Levine, A. Keesling, and M. D. Lukin, “Hardware-efficient, fault-tolerant quantum computation with rydberg atoms,” (2021), arXiv:2105.13501 [quant-ph].
- [35] G. Semeghini, H. Levine, A. Keesling, S. Ebadi, T. T. Wang, D. Bluvstein, R. Verresen, H. Pichler, M. Kalinowski, R. Samajdar, A. Omran, S. Sachdev, A. Vishwanath, M. Greiner, V. Vuletic, and M. D. Lukin, “Probing topological spin liquids on a programmable quantum simulator,” (2021), arXiv:2104.04119 [quant-ph].
- [36] F. M. Surace, P. P. Mazza, G. Giudici, A. Leroise, A. Gambassi, and M. Dalmonte, *Phys. Rev. X* **10**, 021041 (2020).
- [37] A. Celi, B. Vermersch, O. Viyuela, H. Pichler, M. D. Lukin, and P. Zoller, *Phys. Rev. X* **10**, 021057 (2020), arXiv:1907.03311 [quant-ph].
- [38] S. Notarnicola, M. Collura, and S. Montangero, *Phys. Rev. Research* **2**, 013288 (2020).
- [39] X. Wu, X. Liang, Y. Tian, F. Yang, C. Chen, Y.-C. Liu, M. K. Tey, and L. You, *Chin. Phys. B* **30**, 020305 (2021), arXiv:2012.10614 [quant-ph].
- [40] A. Ciavarella, N. Klco, and M. J. Savage, *Phys. Rev. D* **103**, 094501 (2021), arXiv:2101.10227 [quant-ph].
- [41] E. Gustafson, *Phys. Rev. D* **103**, 114505 (2021), arXiv:2104.10136 [quant-ph].

- [42] L. Li and Y. Meurice, *Phys. Rev. D* **71**, 016008 (2005), arXiv:hep-lat/0410029.
- [43] Y. Meurice, *Phys. Rev. D* **80**, 054020 (2009), arXiv:0907.2980 [hep-lat].
- [44] J. Zeiher, R. van Bijnen, P. Schaus, S. Hild, J.-y. Choi, T. Pohl, I. Bloch, and C. Gross, *Nature Physics* **12**, 1095–1099 (2016).
- [45] J. Sakurai, *Modern Quantum Mechanics* (Addison-Wesley, 1994).